Hindawi
Journal of Chemistry
Volume 2023, Article ID 3971686, 10 pages
https://doi.org/10.1155/2023/3971686

Research Article

Biologically Reduced Zinc Oxide Nanosheets Using *Phyllanthus emblica* Plant Extract for Antibacterial and Dye Degradation Studies

Awais Khalid,[1] Pervaiz Ahmad,[2] Mayeen Uddin Khandaker,[3,4] Yosra Modafer,[5] Hanadi A. Almukhlifi,[6] Abdulrahman S. Bazaid,[7] Abdu Aldarhami,[8] Abdulaziz M. Alanazi,[9] Ohoud A. Jefri,[10] Md. Mohi Uddin,[11] and Husam Qanash[7,12]

[1]*Department of Physics, Hazara University Mansehra, Mansehra, Khyber Pakhtunkhwa 21300, Pakistan*
[2]*Department of Physics, University of Azad Jammu and Kashmir, Muzaffarabad 13100, Pakistan*
[3]*Center for Applied Physics and Radiation Technologies, School of Engineering and Technology, Sunway University, Bandar Sunway 47500, Selangor, Malaysia*
[4]*Department of General Educational Development, Faculty of Science and Information Technology, Daffodil International University, DIU Rd, Dhaka 1341, Bangladesh*
[5]*Department of Biology, College of Science, Jazan University, Jazan 45142, Saudi Arabia*
[6]*Department of Chemistry, Faculty of Science, University of Tabuk, Tabuk 71491, Saudi Arabia*
[7]*Department of Medical Laboratory Science, College of Applied Medical Sciences, University of Ha'il, Hail 55476, Saudi Arabia*
[8]*Department of Medical Microbiology, Qunfudah Faculty of Medicine, Umm Al-Qura University, Al-Qunfudah 21961, Saudi Arabia*
[9]*Department of Chemistry, Faculty of Science, Islamic University of Madinah, Madinah 42351, Saudi Arabia*
[10]*Department of Biological Science, Faculty of Science, King Abdulaziz University, Jeddah 21589, Saudi Arabia*
[11]*Department of Physics, Chittagong University of Engineering and Technology (CUET), Chattogram 4349, Bangladesh*
[12]*Medical and Diagnostics Research Centre, University of Ha'il, Hail 55476, Saudi Arabia*

Correspondence should be addressed to Pervaiz Ahmad; pervaiz_pas@yahoo.com and Mayeen Uddin Khandaker; mayeenk@diu.edu.bd

Received 14 December 2022; Revised 10 February 2023; Accepted 18 April 2023; Published 29 April 2023

Academic Editor: Ashanul Haque

The nanostructures synthesized using the green chemistry method have recently attracted the attention of scientists due to their significance in many scientific domains. This work provides an overview of the biosynthesis of zinc oxide (ZnO) nanosheets (NSs) using *Phyllanthus emblica* plant (PEP) extract. X-ray diffraction analysis (XRD), X-ray photoelectron spectroscopy (XPS), scanning electron microscopy (SEM), and Fourier transform infrared (FTIR) were used to analyze the synthesized ZnO-NSs. Evaluation of the antibacterial activity of biosynthesized ZnO-NSs was performed. ZnO-NSs exhibit effective antibacterial activity against Gram-positive (*S. pyogenes* and *S. aureus*) and Gram-negative (*S. typhi* and *E. coli*) bacterial strains. *S. typhi* is the most sensitive microbe towards ZnO-NSs and formed a 21 mm zone of inhibition (ZOI). ZnO-NSs are also tested as a photocatalyst in the degradation of methyl orange (MO) and rhodamine B (RB). The degradation rate of MO was 90%, and RB was 96% after being exposed to UV light for 120 min. The as-synthesized ZnO-NSs exhibited selective dye degradation and showed relatively better photocatalytic activity for positively charged (cationic) dyes. This work could lead to the fabrication of high-yield photocatalysts, which have the potential to degrade textile dyes from aqueous solution.

1. Introduction

Nanotechnology is considered a developing field in science and technology. It has been playing a crucial role in the development of various nanomaterials in recent years. Numerous advantages of pharmaceutical nanoparticles have grabbed the attention of many researchers for innovations [1]. The prevalence of infections that are resistant to antibiotic treatment has prompted a constant quest for new substitutes [2]. Water-borne bacteria species constitute a serious hazard to public health among drug-resistant pathogens because they cause the spread of illnesses such as diarrhea [3]. A variety of pathogenic bacterial species have shown inorganic nanoparticles to be poisonous [4, 5]. The bactericidal impact of inorganic nanoparticles is poorly understood, even though their broad-spectrum biocidal action is well documented [6, 7]. It has been suggested that when ions are released into a solution, reactive oxygen species are generated that are harmful to bacteria [8]. Other studies indicated that due to their small size, nanoparticles could enter the cell wall of bacteria and damage organelles, which results in cell death [9, 10]. In contrast to their organic counterparts, inorganic antibiotics have multiple targets [11, 12].

Zinc oxide is considered a quite interesting material because of its application in areas such as optical, endodontics, and gas sensing. In addition, zinc oxide has been considered an antifungal agent which has no toxicity and harmful environmental effects [13–15]. Due to the safety of zinc oxide nanoparticles and their compatibility with human skin, it is accepted as an additive for textiles and surfaces that meet human skin [16]. ZnO nanoparticles express high photocatalytic properties, which enhances their antifungal activity [17, 18]. ZnO nanoparticles produce ROS under UV light. The primary uses of zinc oxide in the chemical, cosmetics, and pharmaceutical sectors are for its photocatalytic and antibacterial properties [19]. Zinc oxide nanoparticles' antibacterial capabilities have been widely investigated [20, 21], and the development of oxidative stress linked to the particles' photocatalytic activity is thought to be the main cause of toxicity [22]. ZnO is a potential water purification product due to its antiseptic characteristics [23–27].

The plant *Phyllanthus emblica,* commonly identified as Indian gooseberry, grows in areas of Indonesia, India, China, and the Malay Peninsula that are tropical and subtropical. Emblica is one of the most significant herbs in the conventional Ayurvedic medical system and has excellent antioxidant properties. Other conventional medical systems employ it for its immunomodulatory, hepatoprotective, antiulcer, anti-inflammatory, and anticancer effects. Flavonoids, gallic acid [24], kaempferol, pyrogallol, ellagic acid, elaeocarpusin, nor sesquiterpenoids, geraniin, corilagin, and prodelphinidins B1 and B2 are some of this plant's chemical components. Plants that have been reported to produce ZnO NPs through biosynthesis are *Citrus aurantifolia* [28], *Calotropis gigantea* [29], *Ocimum tenuiflorum* [30], *Tamarindus indica* [31], Maple leaf [32], *Phyllanthus niruri* [23], *Solanum nigrum* [21], and *Anisochilus carnosus* [22]. Green synthesis of nanomaterials has recently been performed using microbes and plant extract that have been reported to produce ZnO-NSs due to their accessibility, affordability, nontoxic nature, biodegradability, and environmentally friendly qualities.

In this study, ZnO with nanosheets (NSs) like morphology has been synthesized using a green approach. Zinc nitrate and *Phyllanthus emblica* leaves extract were used to prepare ZnO-NSs. XRD, XPS, SEM, FTIR, and UV spectrophotometer were used to analyze the prepared NSs. Studies have also been carried out to analyze the antibacterial and photocatalytic efficiency of ZnO-NSs. Several methods were reported to synthesize ZnO, but no one in the literature claims to synthesize ZnO-NSs using *Phyllanthus emblica* plant leaves extract.

2. Material and Methods

2.1. Preparation of Zinc Oxide Using Phyllanthus emblica Leaves Extract. Freshly collected PE leaves were washed using distilled water to eliminate any dust, and after that, they were dried at room temperature. A mortar and pestle were used to convert the dried leaves into fine powder. 10 grams of fine powdered PE were added to 100 ml of deionized water under stirring. The subsequent mixture was poured into 0.05 M $ZnCl_2$ solution under continuous stirring on a magnetic hot plate at 90°C for 2 hours. The yellow-colored precipitate was obtained and cooled down to room temperature. To remove the impurity contents, this extract was then centrifuged for 15 minutes at 1000 rpm. The precipitate was continually washed in methanol and distilled water before being dried at 80°C. Finally, at 650°C, the product was calcined for roughly 3 hours in a muffle furnace. The complete synthesis procedure of ZnO using PE extract is shown in Figure 1.

2.2. Characterization. The authors used SEM (MAIA3 TESCAN) to study the physical appearance of ZnO, XRD (Bruker D8 (Germany) was employed to study crystallographic structure, FTIR (Nicolet Avatar 370) was used to analyze the attached functional groups, and chemical composition of synthesized material is studied using XPS Kratos Axis Ultra DLD apparatus (Manchester, UK).

2.3. Antimicrobial Assay. The efficiency of the prepared nanomaterials to inhibit human pathogens was evaluated against microorganisms using the disc diffusion method [26]. Gram-negative pathogenic strains of *E. coli* (ATCC® 33876), *S. typhimurium* (ATCC® 14028), and Gram-positive pathogenic strains of *S. aureus* (ATCC® 11632) and *S. pyogenes* (ATCC® 19615) were employed. To ensure that the nanoparticles were distributed uniformly, 20 mg of the prepared samples were used to make dilution in 1 ml of deionized water. After adding nutrient agar and allowing it to settle, the sterilized Petri plates were inoculated with Gram-negative and Gram-positive bacteria. The solid agar was covered with discs of Whatman filter paper, size 6 mm. At 37°C, nutritional broth was added to all the strains for 18 to 24 hours. The sterile cotton swabs were used to make

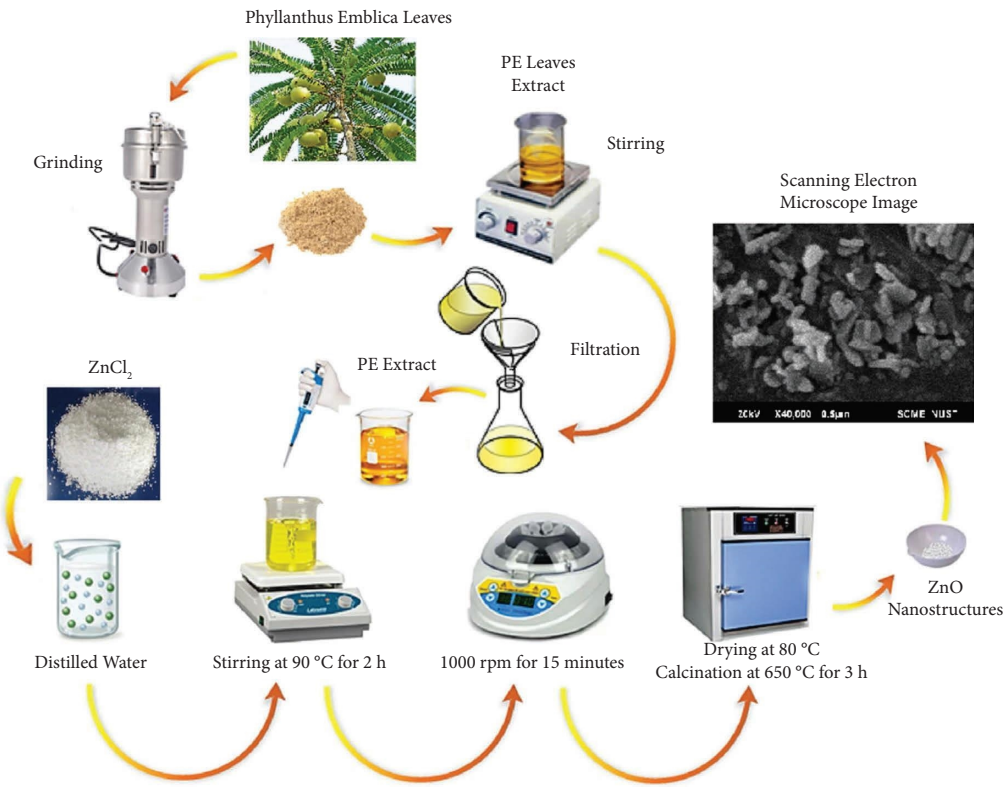

Figure 1: The schematic diagram for the complete synthesis procedure of ZnO-NSs.

streaks across the Muller Hinton agar (MHA) surface. The extract (20 μL) was pipetted onto a sterile paper disc 6 mm in diameter. As a standard reference antibiotic/control, discs containing 40 μl/mL of ciprofloxacin, were employed. Moreover, the plates were placed in an incubator and subjected to incubation at 37°C for 24 h after the solvent had evaporated. The development of a clean zone around the discs is proof that the test sample has antibacterial properties. Using an antibiotic zone scale, the diameter of the inhibition zones was assessed. There were three repetitions for each experiment.

2.4. Photocatalytic Activity Measurement. ZnO nanoparticles' photocatalytic activity was calculated based on the rate at which methylene orange (MO) and rhodamine B (RB) was oxidized when exposed to UV light. Before illumination, both MO and RB dyes (10 ppm) were mixed for 30 min in the dark with the required amount of catalyst (0.5 g). UV-visible spectrophotometer was used at various time intervals to observe the reaction's progress. The color of reaction mixtures progressively faded until it eventually became colorless. An indication of the successful catalytic activity of ZnO was the absorbance for MO and RB measured with a UV-vis spectrometer.

3. Result and Discussion

3.1. Scanning Electron Microscopy (SEM). The morphological features of the synthesized material were investigated through SEM. The obtained images of the ZnO sample showed square-shaped nanosheets with significant particle aggregation, as shown in Figure 2. ZnO-NSs are comparatively homogeneous due to the regular dispersal of Zn cations within a three-dimensional structure. The cluster (agglomeration) in the sample is a result of increased density carried on by the small gap between the particles, while it may also be related to the rapid grain development and nucleation at higher temperatures.

3.2. Structural Analysis. Phase and structural analysis of ZnO NPs prepared using *Phyllanthus emblica* is carried out by XRD analysis and shown in Figure 1. All marked diffraction peak positions in Figure 3 are well matched with the standard JCPDS Card: 36-1451. The corresponding X-ray diffraction peaks at observed planes (100), (002), (101), (102), (110), (103), (200), (112), (201), and (004) confirm the formation of hexagonal wurtzite structure of ZnO. The diffraction peaks' observed line broadening is proof that the produced ZnO NPs are in the nanoscale range. Major peaks' increasing full width at half maxima (FWHM) supports the decline in crystallite size. Using the Scherrer formula, the average crystallite size of ZnO-NSs is determined from the X-ray line broadening.

$$D = \frac{k\lambda}{\beta \cos \theta}. \quad (1)$$

D and λ represent the crystallite size and radiation's wavelength (1.5406 for Cu $k\alpha$), β is the peak intensity width at half maximum, θ is the peak position, and k is a constant

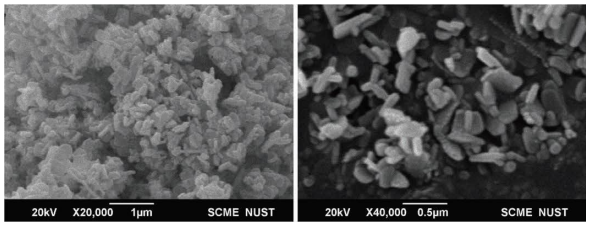

Figure 2: SEM micrographs for ZnO nanosheets synthesized using *Phyllanthus emblica* extract.

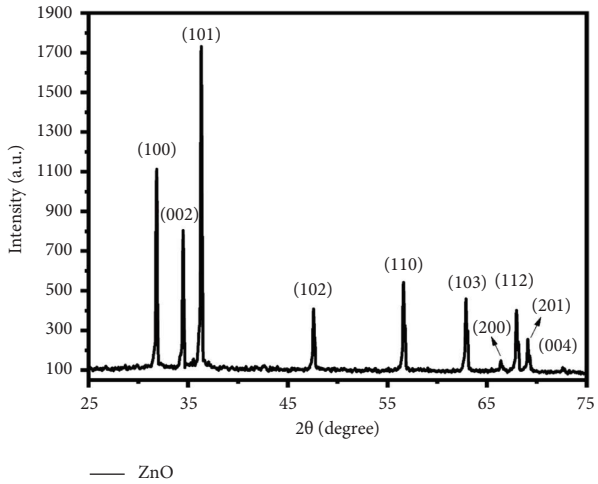

Figure 3: Structural analysis of ZnO-NSs using X-ray photoelectron spectroscopy.

(0.94). The synthesized ZnO-NSs have an average crystallite size of 31 nm.

The Williamson–Hall method was used to determine the lattice strain and crystallite size of ZnO, as shown in Figure 4.

$$\beta \cos \theta = k\lambda D + 4\varepsilon \operatorname{Sin} \theta, \quad (2)$$

where β, D, and ε in the above equation represent full width at half maximum (FWHM), crystallite size, and strain, respectively. The strain is obtained from the linear fit of the data while plotting $\beta \cos \theta$ against $4 \sin \theta$. In comparison to the Williamson–Hall method, which measures crystallite sizes using microstrain, the Scherrer method measures crystallite sizes using the X-rays cohesion length. Any vacancies and defects will make the observed size to be smaller than the actual size.

3.3. Elemental and Chemical State Analysis. To identify the constituent elements of the compound synthesized and examine the sample's surface, a surface-sensitive XPS analysis was conducted. Surface scanning was performed to get the survey spectrum, which provides information about the elemental content of the sample surface, as shown in Figure 5(a). Zn and O are recognized with their corresponding distinctive peaks in a low-resolution spectrum (survey analysis). All samples underwent charge shift correction using the adventitious carbon peak binding energy (284.6 eV). High-resolution spectra of the relevant elements

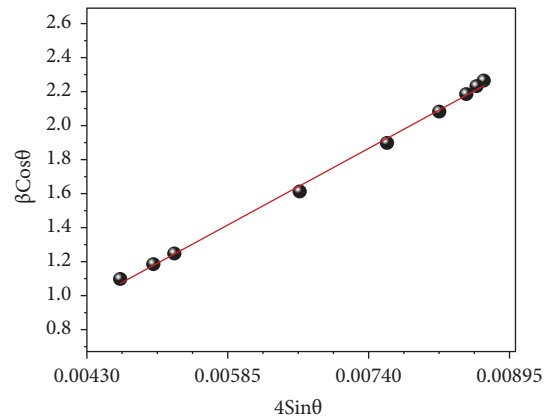

Figure 4: Williamson–Hall plot for ZnO-NS.

were examined in the chemical state study. After laser fragmentation, we carried out high-resolution scanning of the sample. Due to spin-orbital coupling, high-resolution spectra of transition metals such as zinc will exhibit a doublet. Zn thus had doublets for the sample examined in this study. These doublets, which are known as $2p_{3/2}$ and $2p_{1/2}$, represent 2p orbitals. Figures 5(b) and 5(c) show the high-resolution spectra of the materials following laser fragmentation, namely the ZnO sample for Zn 2p and O 1s. The binding energies that are displayed are those that match the primary peak, $Zn2p_{3/2}$. The energy difference between the Zn 2p doublets was 23.1 eV for all samples, which is consistent with previous research [33]. The Zn^{2+} oxidation state is indicated by Zn 2p binding energies in the range of 1022 eV [34]. Pure metallic oxides were chemically represented in the ZnO XPS spectra.

3.4. Fourier Transform Infrared. FTIR spectra of ZnO-NSs produced using the green method were captured in the 500–4000 cm^{-1} range, as shown in Figure 6. The vibrations of the H-O-H bending and O-H stretching were believed to be responsible for the peaks in 1734 and 3418 cm^{-1}, respectively. This demonstrates that the nanocrystalline ZnO contains a little amount of H_2O. The sample was calcined at 400°C for 3 hours, although not all the adsorbed OH groups were removed. The peak in the range of 1451–1734 cm^{-1} was linked to the stretching mode of the C=O group, whereas the band at 847 cm^{-1} corresponds to the vibrations of deformation and elongation of the vibratory Zn-O in ZnO [35].

3.5. Antibacterial Activity. According to numerous studies [36, 37], varying particle morphologies have a considerable impact on ZnO's antibacterial efficacy. This morphology-dependent behavior can be addressed considering the percentage of active aspects on the NPs. Nanomaterial studies have been encouraged, to produce specific nanosized ZnO for antibacterial measurements [38]. The antibacterial activity is also significantly influenced by the concentration and particle size. Research findings have shown that the harmful effect of NPs on microorganisms increases with

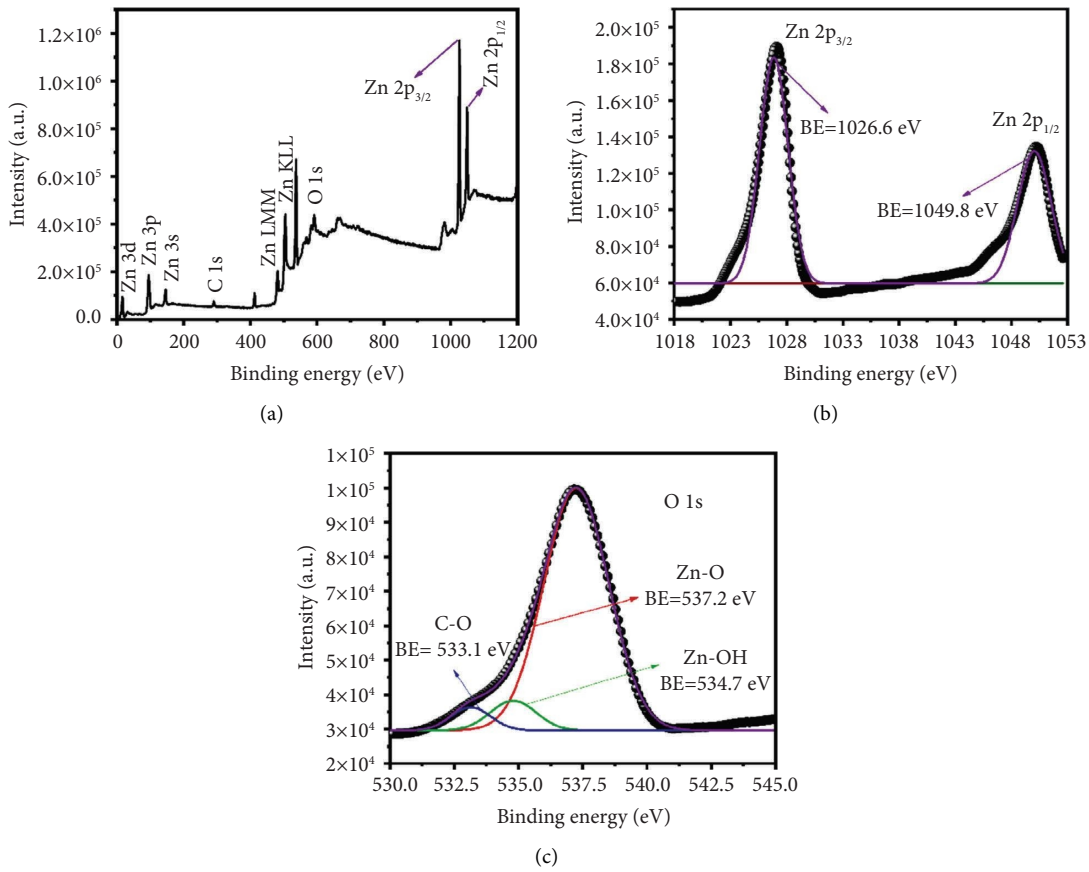

Figure 5: X-ray photoelectron spectroscopic micrographs for (a) survey scan and (b, c) high-resolution spectra for Zn 2p and O 1s.

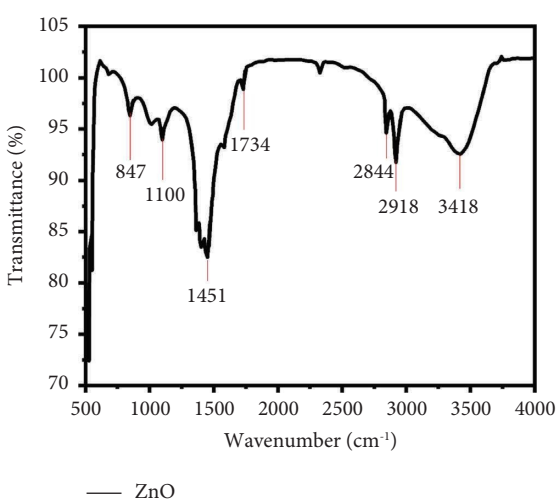

Figure 6: FTIR spectra of ZnO-NSs using *Phyllanthus emblica* extract.

decreasing NP size [39, 40]. Smaller NPs are more effective in penetrating bacterial membranes due to their smaller size and larger contact area [41–43]. The ZnO-NSs employed in this study were prepared using a green chemistry approach and shaped like nanosheets with an average length of 97.2 nm.

The microbial sensitivity of ZnO-NSs fluctuates with the microorganisms and the concentrations of the ZnO-NSs. A zone of inhibition is formed for measured values of 30 μg/mL, 50 μg/mL, and 100 μg/mL. The disc diffusion method was used to test the antibacterial activity of ZnO-NSs against diverse microbes, as shown in Figure 7. Antibacterial activity of pure ZnO shows 18 mm, and 21 mm of inhibition zone for *E. coli* (ATCC® 33876) and *S. Typhimurium* (ATCC® 14028) while for *S. aureus* (ATCC® 11632), *S. pyogenes* (ATCC® 19615) ZnO shows 17 mm and 18 mm of inhibition zone as demonstrated in Table 1 and Figure 8. The inhibition zone indicates the sensitivity of the bacteria to toxic substances, resulting in large inhibition diameters for disinfectant-sensitive pathogens and smaller or even no inhibition diameters for resistant pathogens. Our findings demonstrate that ZnO-NSs can only effectively inhibit bacteria at concentrations of 100 μg/mL or above. This validates that greater volume and concentration result in improved antibacterial action.

3.6. Dye Degradation Study. The factors that affect the photocatalytic dye degradation efficiency of ZnO-based materials are large surface area, particle size, and the presence of functional groups on the surface [44, 45]. ZnO's surface area and photodegradation abilities are improved when its size is reduced. Figures 9(a) and 9(b) show the degradation of MO and RB over time under UV light

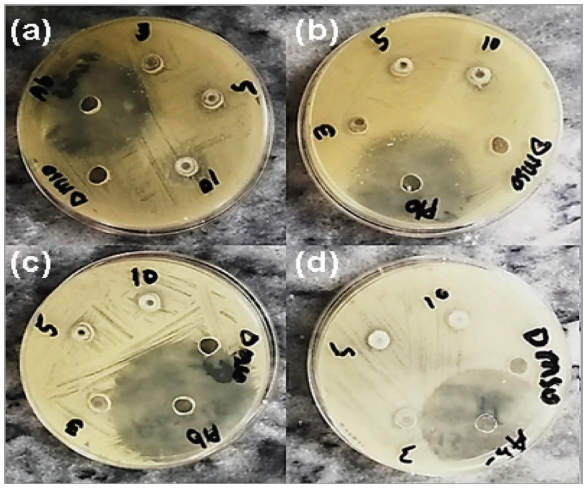

Figure 7: Petri plates containing ZnO-NSs employed against microorganisms using disc diffusion method (a) *S. typhi*, (b) *E. coli*, (c) *S. pyogenes*, and (d) *S. aureus*.

Table 1: Information zone of inhibition formed against bacterial isolates.

Bacteria		30 μg/mL	50 μg/mL	100 μg/mL
E. coli	Inhibition zone (mm)	14 ± 0.28	15 ± 0.36	18 ± 0.34
S. typhimurium		15 ± 0.3	16 ± 0.34	21 ± 0.38
S. aureus		13 ± 0.26	14 ± 0.48	17 ± 0.3
S. pyogenes		9 ± 0.18	12 ± 0.4	18 ± 0.32

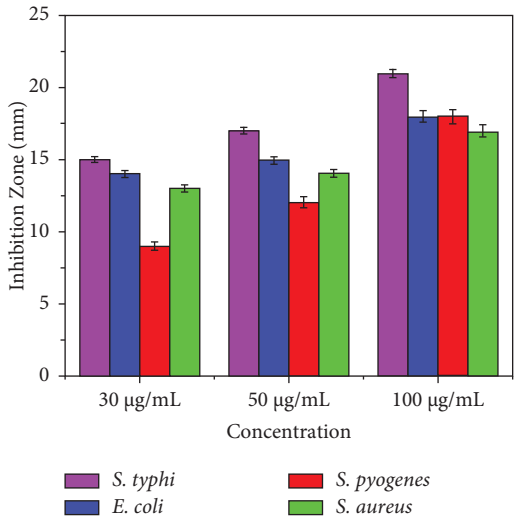

Figure 8: Inhibition zone of microorganisms formed using ZnO-NSs synthesized by PE extract.

irradiation in the presence of ZnO-NSs. The relative intensity of UV-visible spectra was used to determine the amount of dye degradation. The MO and RB dyes were kept in the dark for 20 min before exposure to UV light. No change was observed in the absorption behavior of the dyes in the dark before exposure to UV light. The findings showed that the maximum absorbance of MO and RB dye solution occurs at 481 nm and 563 nm, and constantly decreases when the UV irradiation time is increased. This indicates that ZnO may have accelerated dye degradation with increasing UV exposure time. The degradation % of RB and MO is shown in Figures 10(a) and 10(b); it is observed that the degradation % progressively increased, and about 96% of RB dye and 90% of MO dye degraded within two hours. The kinetics of the photodegradation of organic dyes using ZnO-NSs photocatalyst can be described by several models,

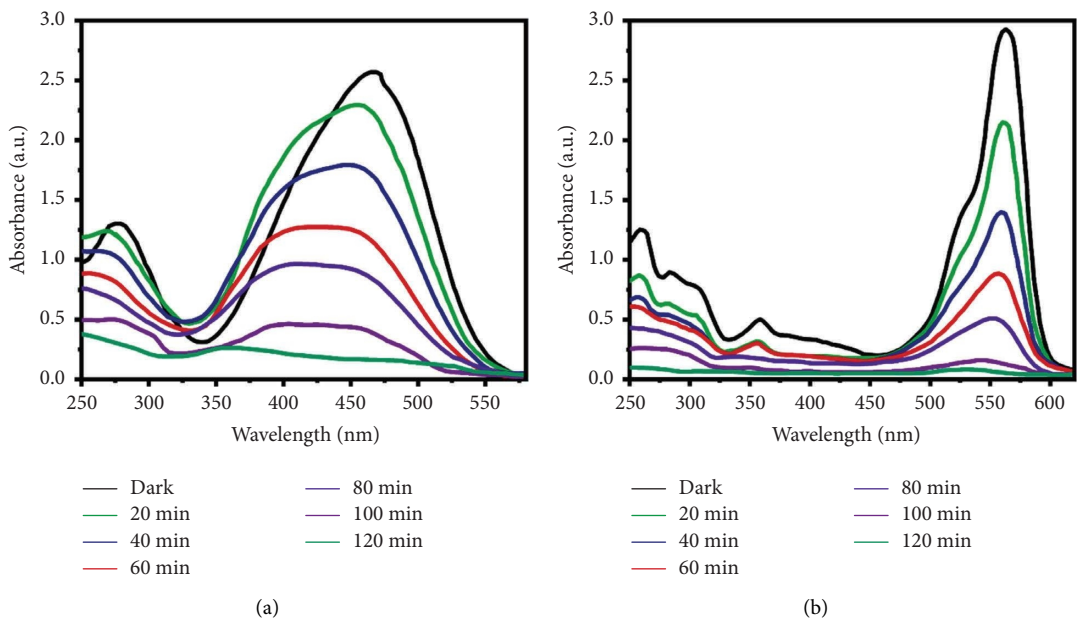

Figure 9: The photocatalytic dye degradation efficiency of ZnO-NSs against (a) methyl orange (MO) and (b) rhodamine B (RB) dyes.

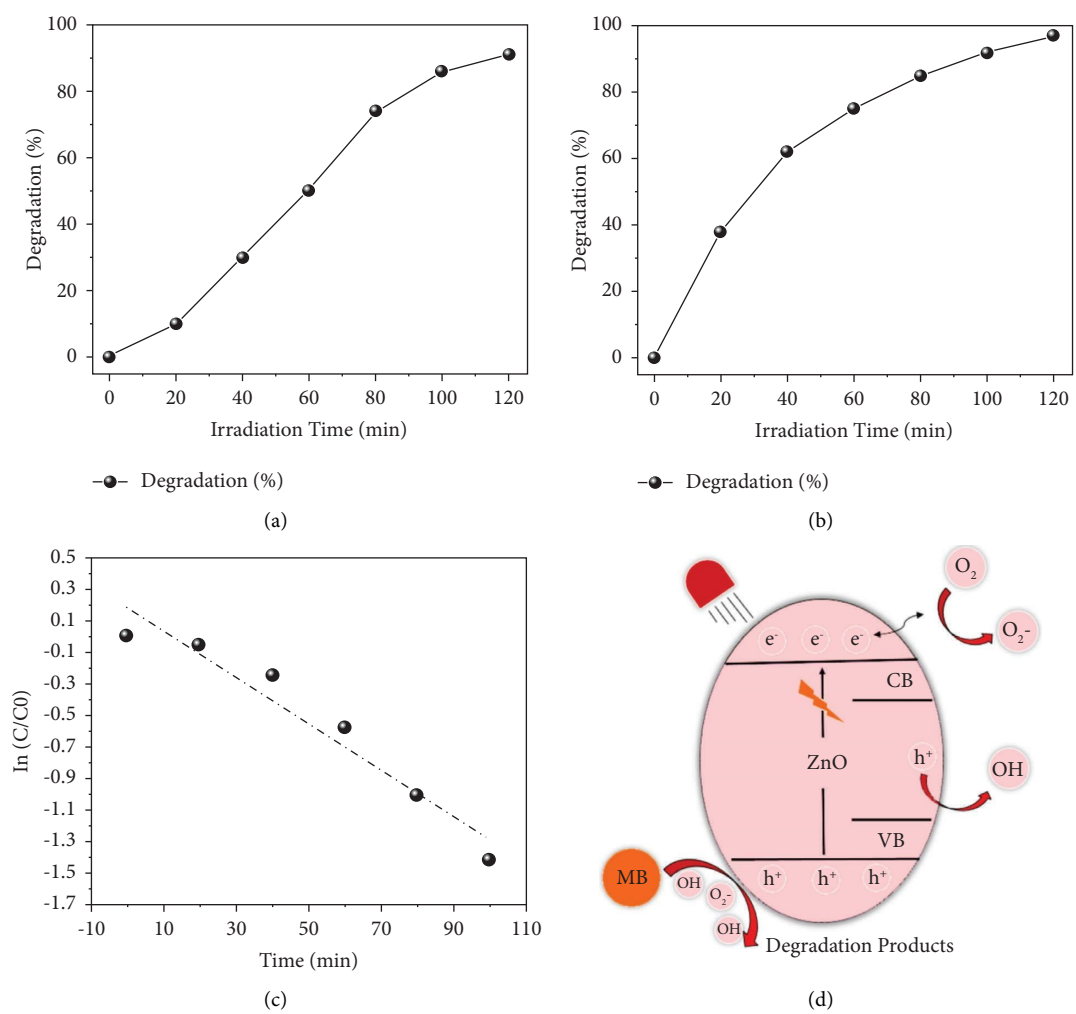

Figure 10: Degradation time versus time of exposure graph for (a) MO, (b) RB dyes using ZnO-NSs, (c) pseudo-first-order kinetics, and (d) schematic illustration for charge transportation process of ZnO-NSs.

including the pseudo-first-order kinetics model and the pseudo-second-order kinetics model [46]. These models are based on the observation that the rate of degradation of RB is dependent on the concentration of both RB and ZnO-NSs. By understanding the kinetics of the photo degradation process, it is possible to optimize the conditions for the efficient removal of MB using ZnO photocatalyst. The rate of degradation calculated using the pseudo-first-order kinetics and schematic illustration for the charge transportation process of ZnO-NSs is shown in Figures 10(c) and 10(d).

4. Conclusion

Green leaf extract from the *Phyllanthus emblica* plant was used to successfully prepare ZnO-NSs, which demonstrates its efficiency as an environmentally friendly, nontoxic, and cost-effective technique to synthesize nanomaterials. The PE extracts employed in the production of nanoparticles act as capping and reducing agents. By using the disc diffusion method, the antibacterial activity of produced nanomaterial was analyzed. It was discovered that ZnO-NSs had a larger zone of inhibition for *S. typhi* (21 mm) than all other tested microbes. The growth and survival curves found in this study help us better understand how ZnO NPs work to kill microorganisms over time. Finally, the findings of this study indicate that some of the most severe and prominent food-borne pathogens can be successfully inhibited when ZnO-NSs prepared from PE extract are used as an antibacterial agent in food systems. The comparative dye degradation studies revealed that the catalysts were able to degrade both rhodamine B (cationic) and methyl orange (anionic) dyes. Rhodamine B (RB) and methyl orange (MO) were degraded by ZnO photocatalyst with the highest efficiency of 96% and 90%, respectively, in 120 minutes. Results suggest that many other hazardous organic compounds that are present in both commercial and residential water resources can also be photodegraded using a ZnO photocatalyst.

Data Availability

All data used in the findings of this study are included within the manuscript.

Conflicts of Interest

The authors declare that they have no conflicts of interest.

Acknowledgments

The authors extend their appreciation to the Higher Education Commission of Pakistan (HEC) for providing funds for our research work under the National Research Program for Universities (NRPU) Project no. 10928. Sunway University International Research Networks Grant Scheme 2.0, STR-IRNGS-SET-CAPRT-01-2022 is acknowledged.

References

[1] H. Agarwal, S. Soumya, and S. Rajeshkumar, "Mechanistic study on antibacterial action of zinc oxide nanoparticles synthesized using green route," *Chemico-Biological Interactions*, vol. 286, pp. 60–70, 2018.

[2] P. Pandey, M. S. Packiyaraj, H. Nigam, G. S. Agarwal, B. Singh, and M. K. Patra, "Antimicrobial properties of CuO nanorods and multi-armed nanoparticles against B. anthracis vegetative cells and endospores," *Beilstein Journal of Nanotechnology*, vol. 5, no. 1, pp. 789–800, 2014.

[3] I. A. Ahmed, H. S. Hussein, Z. A. Alothman, A. G. Alanazi, N. S. Alsaiari, and A. Khalid, "Green synthesis of Fe–Cu bimetallic supported on alginate-limestone nanocomposite for the removal of drugs from contaminated water," *Polymers*, vol. 15, no. 5, p. 1221, 2023.

[4] S. Kar, B. Bagchi, B. Kundu et al., "Synthesis and characterization of Cu/Ag nanoparticle loaded mullite nanocomposite system: a potential candidate for antimicrobial and therapeutic applications," *Biochimica et Biophysica Acta (BBA) - General Subjects*, vol. 1840, no. 11, pp. 3264–3276, 2014.

[5] T. Zhang, X. Wu, S. M. Shaheen et al., "Improving the humification and phosphorus flow during swine manure composting: a trial for enhancing the beneficial applications of hazardous biowastes," *Journal of Hazardous Materials*, vol. 425, Article ID 127906, 2022.

[6] G. Franci, A. Falanga, S. Galdiero et al., "Silver nanoparticles as potential antibacterial agents," *Molecules*, vol. 20, no. 5, pp. 8856–8874, 2015.

[7] A. A. Abdellatif, H. N. Alturki, and H. M. J. Tawfeek, "Different cellulosic polymers for synthesizing silver nanoparticles with antioxidant and antibacterial activities," *Scientific Reports*, vol. 11, no. 1, pp. 84–18, 2021.

[8] A. A. Abdellatif, "Green synthesis of silver nanoparticles incorporated aromatherapies utilized for their antioxidant and antimicrobial activities against some clinical bacterial isolates," *Bioinorganic Chemistry and Applications*, vol. 2022, Article ID 2432758, 14 pages, 2022.

[9] O. Bondarenko, K. Juganson, A. Ivask, K. Kasemets, M. Mortimer, and A. Kahru, "Toxicity of Ag, CuO and ZnO nanoparticles to selected environmentally relevant test organisms and mammalian cells in vitro: a critical review," *Archives of Toxicology*, vol. 87, no. 7, pp. 1181–1200, 2013.

[10] A. Khalid, P. Ahmad, A. I. Alharthi et al., "Structural, optical, and antibacterial efficacy of pure and zinc-doped copper oxide against Pathogenic bacteria," *Nanomaterials*, vol. 11, no. 2, p. 451, 2021.

[11] A. A. Abdellatif, "Silver nanoparticles stabilized by poly (vinyl pyrrolidone) with potential anticancer activity towards prostate cancer," *Synthesis, Characterization, and Applications of Bioinorganic-Based Nanomaterials for Environmental Pollution Hazards*, vol. 2022, Article ID 6181448, 12 pages, 2022.

[12] A. A. Abdellatif, "Green synthesis of silver nanoparticles for enhancing wound healing activity in rats," *Saudi Pharmaceutical Journal*, vol. 10, 2022.

[13] M. Srinisha, "Amla fruit mediated synthesis of zinc oxide nanoparticles and its antifungal activity," *International Journal of Research in Pharmaceutical Sciences*, vol. 10, 2019.

[14] A. Naveed Ul Haq, "Synthesis approaches of zinc oxide nanoparticles: the dilemma of ecotoxicity," *Journal of Nanomaterials*, vol. 2017, Article ID 8510342, 14 pages, 2017.

[15] R. J. I. J. Saraf, "Cost effective and monodispersed zinc oxide nanoparticles synthesis and their characterization," *International Journal of Advances in Applied Sciences*, vol. 2, no. 2, pp. 85–88, 2013.

[16] Q. Liu, M. Zhang, Z. Fang, and X. Rong, "Effects of ZnO nanoparticles and microwave heating on the sterilization and product quality of vacuum packaged Caixin," *Journal of the Science of Food and Agriculture*, vol. 94, no. 12, pp. 2547–2554, 2014.

[17] J. W. Rasmussen, E. Martinez, P. Louka, and D. G. Wingett, "Zinc oxide nanoparticles for selective destruction of tumor cells and potential for drug delivery applications," *Expert Opinion on Drug Delivery*, vol. 7, no. 9, pp. 1063–1077, 2010.

[18] A. Khalid, P. Ahmad, R. Memon et al., "Structural, optical, and renewable energy-assisted photocatalytic dye degradation studies of ZnO, CuZnO, and CoZnO nanostructures for wastewater treatment," *Separations*, vol. 10, no. 3, p. 184, 2023.

[19] R. A. Basit, Z. Abbasi, M. Hafeez et al., "Successive photocatalytic degradation of methylene blue by ZnO, CuO and ZnO/CuO synthesized from coriandrum sativum plant extract via green synthesis technique," *Crystals*, vol. 13, no. 2, p. 281, 2023.

[20] P. K. Stoimenov, R. L. Klinger, G. L. Marchin, and K. J. Klabunde, "Metal oxide nanoparticles as bactericidal agents," *Langmuir*, vol. 18, no. 17, pp. 6679–6686, 2002.

[21] T. Jin, D. Sun, J. Su, H. Zhang, and H. J. Sue, "Antimicrobial efficacy of zinc oxide quantum dots against Listeria monocytogenes, Salmonella enteritidis, and *Escherichia coli* O157: H7," *Journal of Food Science*, vol. 74, no. 1, pp. M46–M52, 2009.

[22] A. Baranwal, "Prospects of nanostructure materials and their composites as antimicrobial agents," *Frontiers In Microbiology*, vol. 9, p. 422, 2018.

[23] A. Khalid, P. Ahmad, A. I. Alharthi et al., "Enhanced optical and antibacterial activity of hydrothermally synthesized cobalt-doped zinc oxide cylindrical microcrystals," *Materials*, vol. 14, no. 12, p. 3223, 2021.

[24] A. Khalid, P. Ahmad, A. Khan et al., "Effect of Cu doping on ZnO nanoparticles as a photocatalyst for the removal of organic wastewater," *Bioinorganic Chemistry and Applications*, vol. 2022, Article ID 9459886, 12 pages, 2022.

[25] A. Sharma, D. Mangla, A. Choudhry, M. Sajid, and S. Ali Chaudhry, "Facile synthesis, physico-chemical studies of Ocimum sanctum magnetic nanocomposite and its adsorptive application against Methylene blue," *Journal of Molecular Liquids*, vol. 362, Article ID 119752, 2022.

[26] A. Sharma, D. Mangla, M. Chaudhry, and S. A. Chaudhry, "Recent advances in magnetic composites as adsorbents for wastewater remediation," *Journal of Environmental Management*, vol. 306, Article ID 114483, 2022.

[27] A. Choudhry, "Origanum vulgare manganese ferrite nanocomposite: An advanced multifunctional hybrid material for dye remediation," *Environmental Research*, vol. 220, Article ID 115193, 2023.

[28] N. A. Samat and R. M. J. C. I. Nor, *Sol–gel synthesis of zinc oxide nanoparticles using Citrus aurantifolia extracts*, vol. 39, pp. S545–S548, 2013.

[29] S. P. J. B. Patil and A. Sciences, "Calotropis gigantea assisted green synthesis of nanomaterials and their applications: a review," vol. 9, no. 1, pp. 1–9, 2020.

[30] S. Sharma, K. Kumar, N. Thakur, and M. S. Chauhan, "Ocimum tenuiflorum leaf extract as a green mediator for the synthesis of ZnO nanocapsules inactivating bacterial pathogens," *Chemical Papers*, vol. 74, no. 10, pp. 3431–3444, 2020.

[31] D. Thatikayala, V. Banothu, J. Kim, D. S. Shin, S. Vijayalakshmi, and J. Park, "Enhanced photocatalytic and antibacterial activity of ZnO/Ag nanostructure synthesized by *Tamarindus indica* pulp extract," *Journal of Materials Science: Materials in Electronics*, vol. 31, no. 7, pp. 5324–5335, 2020.

[32] S. Vivekanandhan, M. Schreiber, C. Mason, A. K. Mohanty, and M. Misra, "Maple leaf (Acer sp.) extract mediated green process for the functionalization of ZnO powders with silver nanoparticles," *Colloids and Surfaces B: Biointerfaces*, vol. 113, pp. 169–175, 2014.

[33] A. Khalid, "Synthesis of boron-doped zinc oxide nanosheets by using phyllanthus emblica leaf extract: a sustainable environmental applications," *Frontiers in Chemistry*, vol. 10, 2022.

[34] A. Khalid, P. Ahmad, A. I. Alharthi et al., "Synergistic effects of Cu-doped ZnO nanoantibiotic against Gram-positive bacterial strains," vol. 16, no. 5, p. e0251082, 2021.

[35] X. Bai, L. Li, H. Liu, L. Tan, T. Liu, and X. Meng, "Solvothermal synthesis of ZnO nanoparticles and anti-infection application in vivo," *ACS Applied Materials & Interfaces*, vol. 7, no. 2, pp. 1308–1317, 2015.

[36] A. Stanković, S. Dimitrijević, and D. Uskoković, "Influence of size scale and morphology on antibacterial properties of ZnO powders hydrothemally synthesized using different surface stabilizing agents," *Colloids and Surfaces B: Biointerfaces*, vol. 102, pp. 21–28, 2013.

[37] N. Talebian, S. M. Amininezhad, and M. Doudi, "Controllable synthesis of ZnO nanoparticles and their morphology-dependent antibacterial and optical properties," *Journal of Photochemistry and Photobiology B: Biology*, vol. 120, pp. 66–73, 2013.

[38] A. Sirelkhatim, S. Mahmud, A. Seeni et al., "Review on zinc oxide nanoparticles: antibacterial activity and toxicity mechanism," *Nano-Micro Letters*, vol. 7, no. 3, pp. 219–242, 2015.

[39] S. Nair, A. Sasidharan, V. V. Divya Rani et al., "Role of size scale of ZnO nanoparticles and microparticles on toxicity toward bacteria and osteoblast cancer cells," *Journal of Materials Science: Materials in Medicine*, vol. 20, no. S1, pp. 235–241, 2009.

[40] O. J. Yamamoto, "Influence of particle size on the antibacterial activity of zinc oxide," *International Journal of Inorganic Materials*, vol. 3, no. 7, pp. 643–646, 2001.

[41] M. Ramani, S. Ponnusamy, C. Muthamizhchelvan, and E. Marsili, "Amino acid-mediated synthesis of zinc oxide nanostructures and evaluation of their facet-dependent antimicrobial activity," *Colloids and Surfaces B: Biointerfaces*, vol. 117, pp. 233–239, 2014.

[42] Z. Razzaq, A. Khalid, P. Ahmad et al., "Photocatalytic and antibacterial potency of titanium dioxide nanoparticles: a cost-effective and environmentally friendly media for treatment of air and wastewater," *Catalysts*, vol. 11, no. 6, p. 709, 2021.

[43] P. Ahmad, A. Khalid, M. U. Khandaker et al., "The antibacterial and antioxidant efficacy and neutron sensing potency of 10B enriched hexagonal boron nitride nanoparticles,"

Materials Science in Semiconductor Processing, vol. 141, Article ID 106419, 2022.

[44] M. Hafeez, S. Afyaz, A. Khalid et al., "Synthesis of cobalt and sulphur doped titanium dioxide photocatalysts for environmental applications," *Journal of King Saud University Science*, vol. 34, no. 4, Article ID 102028, 2022.

[45] A. Khalid, P. Ahmad, A. Khan et al., "Cytotoxic and photocatalytic studies of hexagonal boron nitride nanotubes: a potential candidate for wastewater and air treatment," *RSC Advances*, vol. 12, no. 11, pp. 6592–6600, 2022.

[46] S. Shakeel, F. N. N. Talpur, M. A. Iqbal et al., "Xanthan gum-mediated silver nanoparticles for ultrasensitive electrochemical detection of Hg2+ ions from water," *Catalysts*, vol. 13, no. 1, p. 208, 2023.